coatings

MDPI

Article

Work Function Tuning of Zinc–Tin Oxide Thin Films Using High-Density O_2 Plasma Treatment

Young-Hee Joo [1], Jae-Hyung Wi [1], Woo-Jung Lee [2], Yong-Duck Chung [2,3], Dae-Hyung Cho [2], Saewon Kang [4], Doo-Seung Um [5,*] and Chang-Il Kim [1,*]

1 School of Electrical and Electronics Engineering, Chung-Ang University, Seoul 06974, Korea; ston10000@cau.ac.kr (Y.-H.J.); jaehyungwi@gmail.com (J.-H.W.)
2 Electronics and Telecommunications Research Institute (ETRI), Daejeon 34129, Korea; mirujoa@etri.re.kr (W.-J.L.); ydchung@etri.re.kr (Y.-D.C.); dhcho@etri.re.kr (D.-H.C.)
3 Department of Advanced Device Technology, Korea University of Science and Technology (UST), Daejeon 34113, Korea
4 School of Materials Science and Engineering, Georgia Institute of Technology (GIT), Atlanta, GA 30332, USA; skang359@gatech.edu
5 Department of Electrical Engineering, Sejong University, Seoul 05006, Korea
* Correspondence: dsum@sejong.ac.kr (D.-S.U.); cikim@cau.ac.kr (C.-I.K.)

Received: 15 September 2020; Accepted: 20 October 2020; Published: 25 October 2020

Abstract: Work function tuning has a significant influence on the performance of semiconductor devices, owing to the formation of potential barriers at the interface between metal-semiconductor junctions. In this work, we introduce a technique for tuning the work function of ZnSnO thin films using high-density O_2 plasma treatment. The work function and chemical composition of the ZnSnO thin film surfaces were investigated with regards to plasma treatment time through UPS/XPS systems. The optical band gap was estimated using Tauc's relationship from transmittance data. The work function of $Zn_{0.6}Sn_{0.4}O$ thin film increased from 4.16 eV to 4.64 eV, and the optical band gap increased from 3.17 to 3.23 eV. The surface of $Zn_{0.6}Sn_{0.4}O$ thin films showed a smooth morphology with an average of 0.65 nm after O_2 plasma treatment. The O_2 plasma treatment technique exhibits significant potential for application in high-performance displays in optical devices, such as thin-film transistors (TFTs), light-emitting diodes (LEDs), and solar cells.

Keywords: zinc tin oxide; transparent conductive oxide; work function; O_2 plasma; surface treatment; XPS; UPS

1. Introduction

Particular attention needs to be focused on the device-structure design to improve the efficiencies of electrical and optical devices. Notably, the work function of thin films is directly related to the performances of these devices [1,2]. For example, the difference in the work function between the metal-semiconductor junction at the source (or drain) leads to an increase in contact resistance, resulting in performance degradation of the device [3,4]. Meanwhile, the operation of Schottky diodes, metal–semiconductor–metal photodetectors, and Schottky junction solar cells is based on the difference in work function between the metal-semiconductor junctions [5–7]. It is evident that the characteristics of the electrical and optical devices are closely related to the work function of the materials [8]. Therefore, considering work functions while designing devices is crucial to improve performance. Kang et al. reported an increase in carrier mobility of InGaZnO thin films through Ar plasma treatment [9]. Furthermore, Fang et al. proposed tuning the work function of the InSnO (ITO) thin film through Ar plasma treatment by employing a capacitively coupled plasma system [10]. Plasma

treatment induces oxygen vacancy on the thin film surface and modulates the Sn doping concentration, resulting in the tuning of the work function and improvement of the carrier mobility [11,12].

Zinc–tin oxide ($Zn_{1-x}Sn_xO$) thin films are transparent oxide semiconductors with wide bandgaps (E_g ~ 3.6 eV) and have been studied as potential materials for channel layers in thin-film transistors (TFTs) [13,14], emitters for photovoltaic devices [15], as well as transparent conducting electrodes [16,17]. ZnSnO TFTs exhibit lower carrier mobility than InGaZnO or InZnSnO TFTs, and ZnSnO as transparent electrodes exhibit lower performance than ITO-based electrodes. However, they boast low manufacturing cost and wide functionality as indium-free oxide-based thin films [18–20].

In this work, we present a technique for tuning the work function and electrical properties of ZnSnO thin films through high-density O_2 plasma treatment in an inductively coupled plasma (ICP) system. Depending on the O_2 plasma treatment time, the work function changed from 4.16 to a maximum value of 4.64 eV, while the optical band gap remained steady. Moreover, while the electrical properties were altered during the plasma treatment, there was no significant change observed in surface roughness.

2. Materials and Methods

A 100 nm $Zn_{0.6}Sn_{0.4}O$ thin film was deposited on soda-lime glass (SLG) by an RF co-sputtering system (SNETEK Co., LTD., Suwon, Korea) with the pure ZnO (99.99%) and Sn (99.99%) metal targets under 100 and 40 W RF power, respectively. The substrate temperature was 200 °C, while an Ar/O_2 mixed gas (90/10%) was injected with a total gas flow rate of 100 sccm. The base and working pressures were maintained at 5.0×10^{-7} Torr and 20 mTorr, respectively. The Sn/(Sn + Zn) ratio was controlled by varying the oxygen partial pressure with fixed sputter power. The deposited-$Zn_{0.6}Sn_{0.4}O$ (60%Zn:40%Sn atomic ratio) thin films were treated with O_2 plasma in the inductively coupled plasma (ICP) system (Vacuum Science, Yangju, Korea) for tuning the work function [21]. During O_2 plasma treatment, the total flow rate of the O_2 gas was fixed at 20 sccm. The RF power, DC bias voltage, process pressure, and substrate temperature were fixed at 500 W, −200 V, 15 mTorr and room temperature, respectively. After O_2 plasma treatment, the surface chemical state and the work function of the $Zn_{0.6}Sn_{0.4}O$ thin films were investigated using X-ray/ultraviolet photoelectron spectroscopy (XPS/UPS). The XPS (K-alpha, Thermo VG, UK) measurements employed a monochromatic Al Kα source (1486.6 eV). The X-ray power, current, and base pressure were 12 kV, 3 mA, and 2.2×10^{-7} Torr, respectively. Here, binding energies were referenced to the neutral C 1*s* peak at 284.6 eV. The UPS (AXIS Ultra DLD, Kratos, Inc., Manchester, UK) measurements were carried out using an He I (21.2 eV) gas discharge lamp. The base pressure and dwell time were 4.0×10^{-8} Torr and 100 ms, respectively. A UV-Vis-NIR spectrophotometer (Perkin elmer, Waltham, MA, US) was used to measure the transmittance and optical band gap (E_g) of the $Zn_{0.6}Sn_{0.4}O$ thin films. A Hall measurement system (Accent Optical Technologies, Bend, OR, US)) was used to measure the resistance, mobility, and carrier concentration with van der Pauw geometry. Atomic force microscopy (AFM) (XE-100, PSIA Inc., Suwon, Korea) was used to determine surface morphology. Topographic images were taken in non-contact mode with *X*-*Y* scanner and *Z* scanner of 1×1 μm^2 and 2 nm, respectively.

3. Results and Discussion

The changes in the work function according to the O_2 plasma treatment time were studied through UPS measurements. Figure 1 shows the UPS spectra of the $Zn_{0.6}Sn_{0.4}O$ thin films, depending on the O_2 plasma treatment time. The binding energy cutoff for secondary electrons and the near-Fermi edge on the $Zn_{0.6}Sn_{0.4}O$ thin films are expressed in Figure 1a,b, respectively. The work function (ø) was calculated using the following equation:

$$ø = hv - E_B \text{ (secondary cutoff)} \quad (1)$$

where $h\nu$ is the photon energy (He I, 21.2 eV) and E_B is the binding energy. The as-deposited $Zn_{0.6}Sn_{0.4}O$ thin film exhibited a work function of 4.16 eV, whereas the $Zn_{0.6}Sn_{0.4}O$ thin films treated with O_2 plasma for 60, 90, 120 and 150 s displayed work functions of 4.35, 4.64, 4.38, and 4.56 eV, respectively. As the O_2 plasma treatment time increased, the binding energy of the valence structure at the surface of $Zn_{0.6}Sn_{0.4}O$ thin films changed, owing to the change in the ionization potential. In other words, during plasma treatment, the SnO component is easily etched away, and oxygen penetrates into the oxygen vacancy on the surface, resulting in an increase in the oxygen concentration on the $Zn_{0.6}Sn_{0.4}O$ surface. This results in a change in the work function and valence band offset (VBO) [22]. Furthermore, the change in the work function could be ascribed to the difference in the chemical state or elemental ratio [23,24]. The irregular trend in the work function for O_2 plasma treatment time between 90 and 120 s can be attributed to the difference in the heat of formation of ZnO (−348.0), SnO (−285), and SnO_2 (−577.63). In other words, up to 90 s of O_2 plasma treatment affects the SnO component while ZnO is mainly affected between 90 and 120 s [25]. Therefore, it was observed that the work function of $Zn_{0.6}Sn_{0.4}O$ thin films with O_2 plasma treatment for 90 s is exceptionally higher than the reference values.

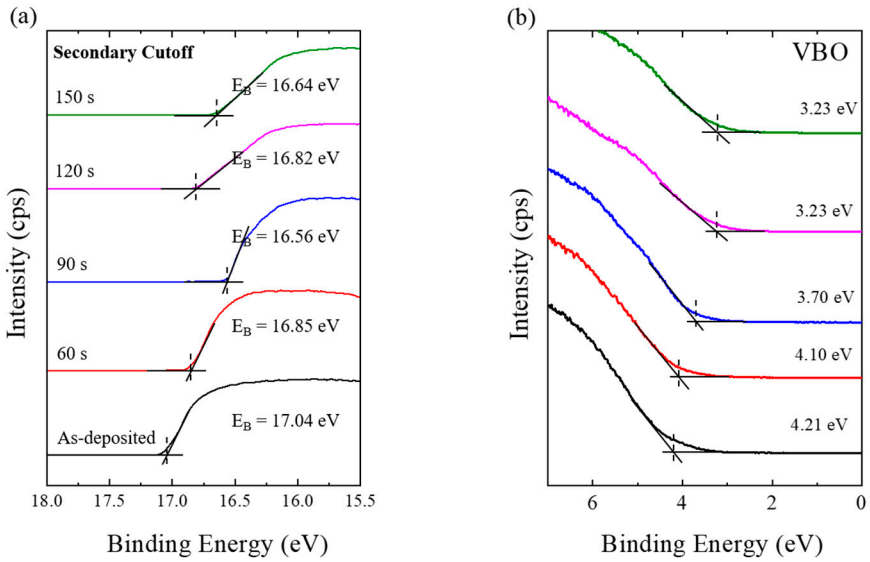

Figure 1. UPS measurements of $Zn_{0.6}Sn_{0.4}O$ thin films exposed to different O_2 plasma treatment times. (**a**) the higher binding energy edge of the secondary electrons and (**b**) the valence structure.

The work function of semiconducting thin films is related to their band gap. We calculated the optical band gap of each $Zn_{0.6}Sn_{0.4}O$ thin film from transmission spectra using, Tauc's relation,

$$(\alpha h\nu)^n = B(h\nu - E_g) \quad (2)$$

where α, B, and E_g are the absorption coefficient, the band tailing parameter, and the optical band gap, respectively. Figure 2 presents the transmission spectra of $Zn_{0.6}Sn_{0.4}O$ thin films depending on the O_2 plasma treatment time. The average transmittance of O_2 plasma-treated $Zn_{0.6}Sn_{0.4}O$ thin films was 92% in the visible region (from 400 to 700 nm). The optical band-gap of the $Zn_{0.6}Sn_{0.4}O$ thin films was calculated to be 3.17 + Δ0.06 eV, based on transmittance data from the Tauc plot (inset image of Figure 2). The band gap was relatively steady with O_2 plasma treatment, while the work function changes were significant.

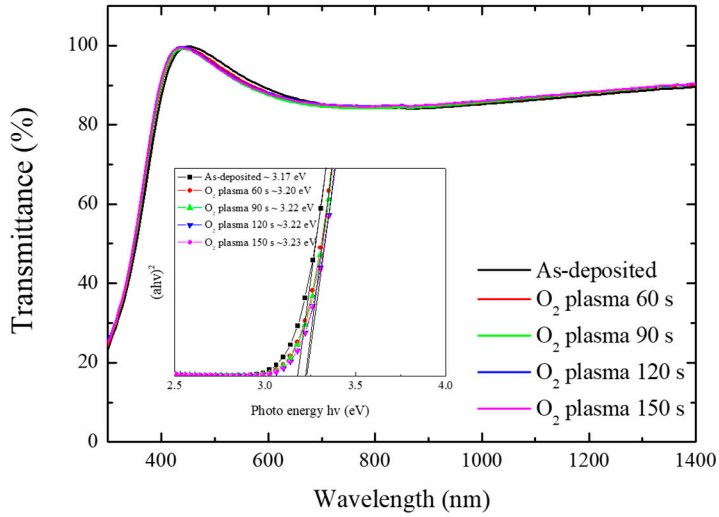

Figure 2. The optical transmittance spectra as a function of O_2 plasma treatment time for the $Zn_{0.6}Sn_{0.4}O$ thin films. In the insert, the magnified spectra of the $Zn_{0.6}Sn_{0.4}O$ thin films and the bandgap of $Zn_{0.6}Sn_{0.4}O$.

Figure 3 shows a schematic of a modified $Zn_{0.6}Sn_{0.4}O$ band position, including work function and band gaps of the O_2 plasma-treated materials. The substituted metal in the ZnO results regarding the movement of the Fermi level toward the conduction band edge with the work function changed [26]. Therefore, the $Zn_{0.6}Sn_{0.4}O$ thin film with the O_2 plasma treatment is comparable with other films for potential applications in high-performance devices, as shown in Figure 3.

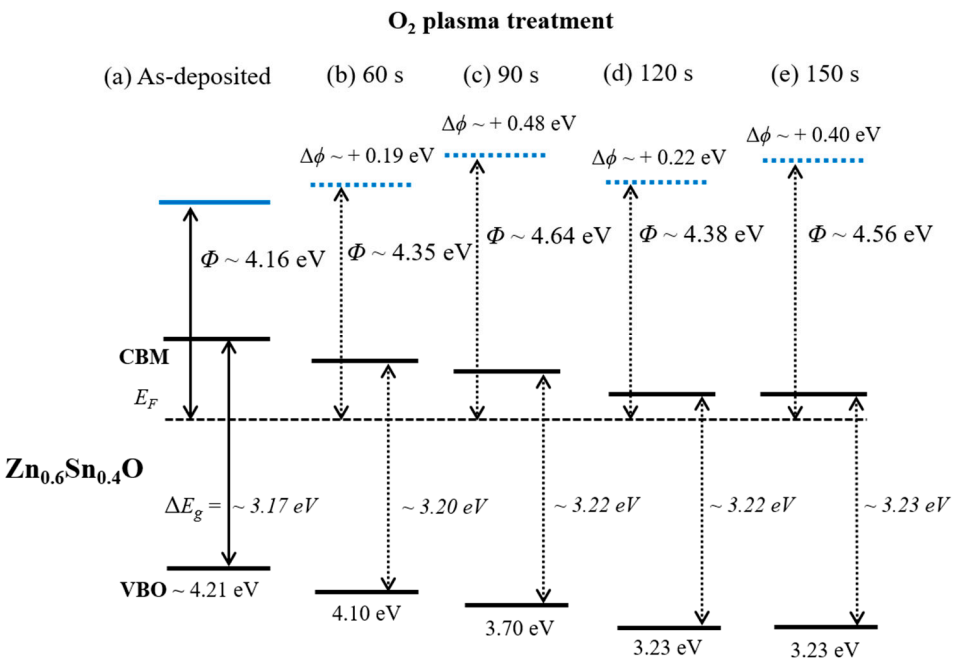

Figure 3. Schematic of modified $Zn_{0.6}Sn_{0.4}O$ band alignment including work functions and band gaps of all of the O_2 plasma treated materials.

Figure 4 shows the changes in the XPS peaks of the $Zn_{0.6}Sn_{0.4}O$ thin films with respect to the O_2 plasma treatment time. The XPS peaks (Zn $2p_{3/2}$, Sn $3d_{5/2}$, and O 1*s*) were deconvoluted for the identification of elements and observation of changes in the composition of the $Zn_{0.6}Sn_{0.4}O$ thin films. In the as-deposited samples, Zn $2p_{3/2}$ core-level spectra were deconvoluted into two main Gaussian components, Zn–OH (1022.58 eV) and Zn–O (1021.78 eV) (Figure 4a) [27–29]. The Sn 3*d* core-level

spectra were also deconvoluted into two Gaussian components, Sn^{2+} (487.08 eV) and Sn^{4+} (486.38 eV), displayed in Figure 4b. The Sn^{2+} and Sn^{4+} oxidation states can lead to p-type SnO and n-type SnO_2 behavior, respectively [30,31]. The O 1*s* sub-peaks corresponding to ZnO (529.6 eV), SnO (531.7 eV), and SnO_2 (530.4 eV) can be attributed to oxidation by reactive sputtering (Figure 4c). The presence of SnO derived components could be attributed to lattice oxygen deficiency and reduced oxygen concentration at the surface [31].

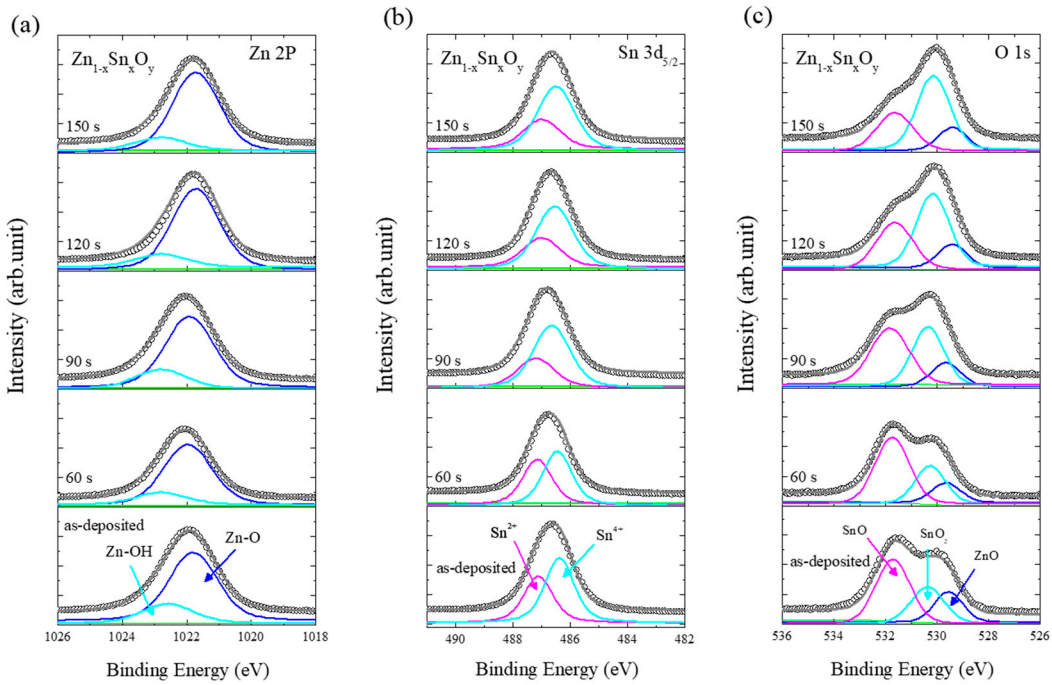

Figure 4. XPS results for Zn 2*p*, Sn 3*d* and O 1*s* core levels as a function of O_2 plasma treatment time for the $Zn_{0.6}Sn_{0.4}O_y$ thin films. (**a**) The Zn $2p_{3/2}$ was deconvoluted with two components for Zn–O and Zn–OH bonds, (**b**) the Sn $3d_{5/2}$ was deconvoluted with two components for Sn^{4+}, and Sn^{2+}, (**c**) the O 1*s* was deconvoluted with three components for SnO, SnO_2, and ZnO bonds.

There was no shift of the Zn 2*p* peak. However, a slight shift of the Sn 3*d* peak was observed, while the O 1*s* peak shifted towards the lower binding energy with increasing O_2 plasma treatment time. Deconvolution analysis of the O_2 plasma treatment time explains the reaction of the O_2 plasma on the surface of the ZnSnO thin film. The Zn–OH related peaks decreased after O_2 plasma treatment from 60 to 150 s (Figure 4a). The O^+ and O^{2+} ions bombard and break the OH–Zn–O or OH–Sn–O bonds during the plasma treatment, resulting in the formation of O_2 or H_2O molecules [22]. The intensity of the Sn^{2+} state decreased dramatically, whereas that of the Sn^{4+} oxidation state remained stable (Figure 4b). This result is attributed to the difference in the Gibbs free energy associated with the formation of SnO and SnO_2 ($\Delta_f G_m(Sn^{2+}, 298.15\ K) = -(27.87 \pm 0.08)\ kJ{\cdot}mol^{-1}$, $\Delta_f G_m\ (Sn^{4+}, 298.15\ K) = (46.7 \pm 3.9)\ kJ{\cdot}mol^{-1}$) [32]. Therefore, SnO bonds are weaker than SnO_2 bonds. The intensity of the ZnO bonding peak remained constant, while the intensities of the SnO_2 and SnO bonding peaks exhibited a consistent increase and decrease, respectively (Figure 4c). This result indicates that ZnO has more ionic characteristics than SnO because Zn is significantly more electropositive than Sn. The equilibrium constant (K_p) of formation for ZnO is higher than that of SnO, because the electrons in Zn are more readily given up than those of Sn [33]. Therefore, the energy required to convert SnO into Sn and O (g) should be lesser than the energy required to convert ZnO into Zn and O (g). The reduction in the Sn^{2+} oxidation state with O_2 plasma treatment (Figure 4b) results in the formation of more n-type SnO_2 in the $Zn_{0.6}Sn_{0.4}O$ thin film, as indicated in Figure 4c.

Figure 5 shows the atomic ratios of the deconvoluted components for Sn^{2+}/Sn^{4+}, SnO/SnO_2, and Zn–OH/Zn–O as a function of O_2 plasma treatment times based on the results of the XPS analysis

in Figure 4. The atomic ratios of Sn^{2+}/Sn^{4+} and SnO/SnO_2 sharply decrease as the O_2 plasma treatment time increases up to 90 s, which then shows a gradual decrease. However, the atomic ratio of Zn–OH/Zn–O shows a sharp decline in the O_2 plasma treatment time between 90 and 120 s.

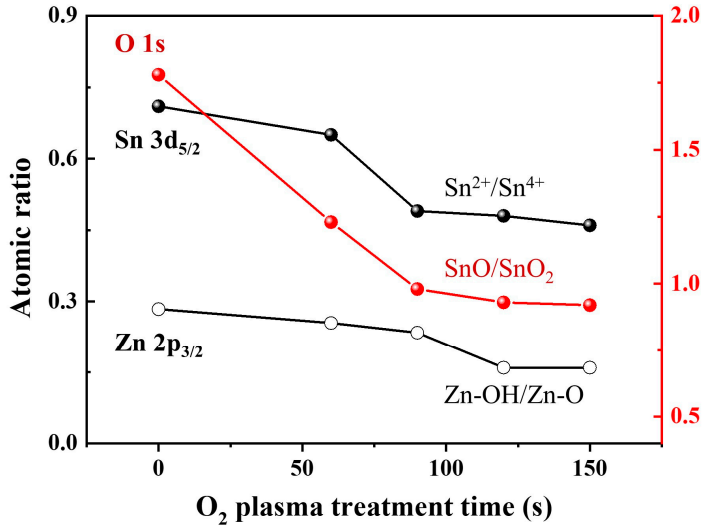

Figure 5. The atomic ratios of the deconvoluted components in the XPS peaks for Sn^{2+}/Sn^{4+}, SnO/SnO_2, and Zn–OH/Zn–O as a function of O_2 plasma treatment time.

Figure 6 shows the resistivity, carrier concentration, and mobility for the $Zn_{0.6}Sn_{0.4}O$ films as a function of O_2 plasma treatment times. As the O_2 plasma treatment time increased up to 90 s, a decrease in resistivity was observed. Meanwhile, the mobility and carrier concentration increased. The lowest resistivity of 2.80×10^{-2} Ω-cm and the highest carrier concentration and mobility of 4.0×10^{19} cm^{-3} and 8.15 $cm^2 \cdot V^{-1} \cdot s^{-1}$, respectively, were achieved at 90 s. However, the resistivity increased and the mobility and carrier concentration decreased as the plasma treatment time increased above 90 s. The O_2 plasma treatment causes a reduction in the Sn/Zn ratio on the $Zn_{0.6}Sn_{0.4}O$ surface. The SnO component in the $Zn_{0.6}Sn_{0.4}O$ film is easily affected until the O_2 plasma treatment reaches 90 s, which increases the carrier concentration at the surface of the film. However, the ZnO component is more easily affected than the SnO component during O_2 plasma treatment between 90 and 120 s (Figure 5), resulting in the increase in the Sn/Zn ratio. In addition, as described for the change in the work function, this sequential effect can be explained by the "heat of formation".

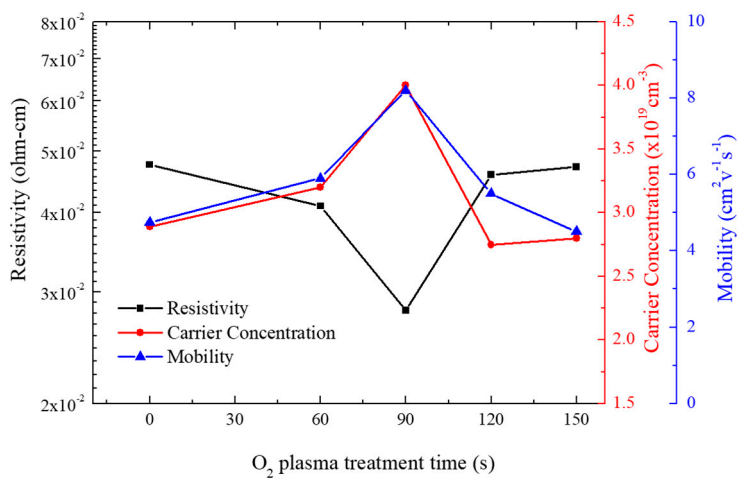

Figure 6. The electrical resistivity, carrier concentration and mobility as a function of O_2 plasma treatment time for the $Zn_{0.6}Sn_{0.4}O$ thin films.

Surface morphology affects the contact resistance at the metal-semiconductor and/or P-N junction [10,34]. Therefore, we employed AFM to investigate the surface properties of $Zn_{0.6}Sn_{0.4}O$ thin films as the O_2 plasma treatment time increased, as shown in Figure 7. The surface roughness (root-mean square, RMS) of the as-deposited $Zn_{0.6}Sn_{0.4}O$ thin film was 0.684 nm and that of the $Zn_{0.6}Sn_{0.4}O$ thin films treated by O_2 plasma for 90 and 150 s were 0.626 and 0.624 nm, respectively. It is evident from these results that the O_2 plasma treatment has no significant effect on the surface roughness.

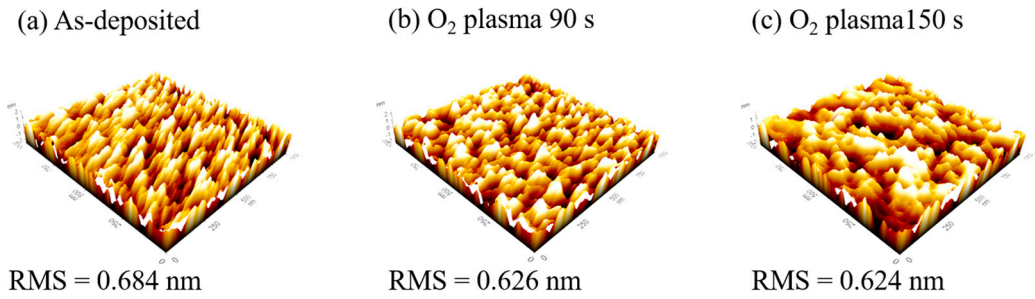

Figure 7. AFM images of the $Zn_{0.6}Sn_{0.4}O$ thin films post O_2 plasma treatment. (**a**) as-deposited, (**b**) 90 s and (**c**) 150 s.

4. Conclusions

In this study, we observed changes in the work function and surface state of $Zn_{0.6}Sn_{0.4}O$ thin film under the influence of high-density O_2 plasma treatment. The work function increased by approximately 0.5 eV (from 4.16 to up to 4.64 eV). However, the change in optical band gap was exceedingly small (3.17 + Δ0.06 eV). The change in work function was ascribed to the change in the surface morphology of the $Zn_{0.6}Sn_{0.4}O$ thin films, inferred from the XPS analysis. In addition, the O_2 plasma treatment resulted in changes in the electrical properties of the thin film, including its resistivity, carrier concentration, and mobility. The mobility significantly increased from 4.75 to 8.2 $cm^2 \cdot V^{-1} \cdot s^{-1}$. Meanwhile, there was no significant change in the surface roughness of the $Zn_{0.6}Sn_{0.4}O$ thin films. In conclusion, we confirmed that the work function and mobility of $Zn_{0.6}Sn_{0.4}O$ thin films can be tuned and improved through O_2 plasma treatment. The O_2 plasma treatment technique exhibits significant potential for application in high-performance displays in optical devices, such as thin-film transistors (TFT), light-emitting diodes (LEDs), and solar cells.

Author Contributions: Conceptualization, Y.-H.J. and J.-H.W.; Methodology, Y.-H.J. and J.-H.W.; Validation, Y.-H.J., J.-H.W., W.-J.L., Y.-D.C., D.-H.C. and S.K.; Data Curation, Y.-H.J., J.-H.W., W.-J.L., Y.-D.C., D.-H.C., S.K. and D.-S.U.; Writing-Original Draft Preparation, Y.-H.J. and J.-H.W.; Writing-Review & Editing, D.-S.U.; Visualization, Y.-H.J. and D.-S.U.; Supervision, D.-S.U. and C.-I.K.; Project Administration, C.-I.K.; Funding Acquisition, C.-I.K. All authors have read and agreed to the published version of the manuscript.

Funding: This research was funded by the National Research Foundation of Korea (NRF) grant funded by the Korea government (MSIT) (No. 2018R1D1A1B07051429).

Acknowledgments: This work supported by the Chung-Ang University Research Scholarship Grants in 2017.

Conflicts of Interest: The authors declare no conflict of interest.

References

1. Ravi, S.K.; Sun, W.X.; Nandakumar, D.K.; Zhang, Y.X.; Tan, S.C. Optical manipulation of work function contrasts on metal thin films. *Sci. Adv.* **2018**, *4*, eaao6050. [CrossRef]
2. Chuang, S.; Battaglia, C.; Azcatl, A.; McDonnell, S.; Kang, J.S.; Yin, X.T.; Tosun, M.; Kapadia, R.; Fang, H.; Wallace, R.M.; et al. MoS_2 P-type transistors and diodes enabled by high work function MoO_x contacts. *Nano Lett.* **2014**, *14*, 1337–1342. [CrossRef]
3. Burgi, L.; Richards, T.J.; Friend, R.H.; Sirringhaus, H. Close look at charge carrier injection in polymer field-effect transistors. *J. Appl. Phys.* **2003**, *94*, 6129–6137. [CrossRef]

4. Dominguez, M.A.; Alcantara, S.; Soto, S. Physically-based simulation of zinc oxide thin-film transistors: Contact resistance contribution on density of states. *Solid-State Electron.* **2016**, *120*, 41–46. [CrossRef]
5. Liang, S.; Sheng, H.; Liu, Y.; Huo, Z.; Lu, Y.; Shen, H. ZnO Schottky ultraviolet photodetectors. *J. Cryst. Growth* **2001**, *225*, 110–113. [CrossRef]
6. Goykhman, I.; Sassi, U.; Desiatov, B.; Mazurski, N.; Milana, S.; de Fazio, D.; Eiden, A.; Khurgin, J.; Shappir, J.; Levy, U.; et al. On-chip integrated, silicon–graphene plasmonic schottky photodetector with high responsivity and avalanche photogain. *Nano Lett.* **2016**, *16*, 3005–3013. [CrossRef]
7. Alnuaimi, A.; Almansouri, I.; Saadat, I.; Nayfeh, A. High performance graphene-silicon Schottky junction solar cells with HfO_2 interfacial layer grown by atomic layer deposition. *Sol. Energy* **2018**, *164*, 174–179. [CrossRef]
8. Lee, K.H.; Jang, H.W.; Kim, K.B.; Tak, Y.H.; Lee, J.L. Mechanism for the increase of indium-tin-oxide work function by O_2 inductively coupled plasma treatment. *J. Appl. Phys.* **2004**, *95*, 586–590. [CrossRef]
9. Kang, J.H.; Cho, E.N.; Kim, C.E.; Lee, M.J.; Lee, S.J.; Myoung, J.M.; Yun, I. Mobility enhancement in amorphous InGaZnO thin-film transistors by Ar plasma treatment. *Appl. Phys. Lett.* **2013**, *102*, 222103. [CrossRef]
10. Fang, M.; Zhang, C.M.; Chen, Q. Tuning the ITO work function by capacitively coupled plasma and its application in inverted organic solar cells. *Appl. Surf. Sci.* **2016**, *385*, 28–33. [CrossRef]
11. Jain, V.K.; Kumar, P.; Kumar, M.; Jain, P.; Bhandari, D.; Vijay, Y.K. Study of post annealing influence on structural, chemical and electrical properties of ZTO thin films. *J. Alloy. Compd.* **2011**, *509*, 3541–3546. [CrossRef]
12. Chandra, R.D.; Rao, M.; Zhang, K.K.; Prabhakar, R.R.; Shi, C.; Zhang, J.; Mhaisalkar, S.G.; Mathews, N. Tuning electrical properties in amorphous zinc tin oxide thin films for solution processed electronics. *ACS Appl. Mater. Interfaces* **2014**, *6*, 773–777. [CrossRef]
13. Chiang, H.Q.; Wager, J.F.; Hoffman, R.L.; Jeong, J.; Keszler, D.A. High mobility transparent thin-film transistors with amorphous zinc tin oxide channel layer. *Appl. Phys. Lett.* **2005**, *86*, 013503. [CrossRef]
14. Heineck, D.P.; McFarlane, B.R.; Wager, J.F. Zinc tin oxide thin-film-transistor enhancement/depletion inverter. *IEEE Electron Device Lett.* **2009**, *30*, 514–516. [CrossRef]
15. Lindahl, J.; Watjen, J.T.; Hultqvist, A.; Ericson, T.; Edoff, M.; Torndahl, T. The effect of $Zn_{1-x}Sn_xO_y$ buffer layer thickness in 18.0% efficient Cd-free $Cu(In,Ga)Se_2$ solar cells. *Prog. Photovolt.* **2014**, *21*, 1588–1597. [CrossRef]
16. Choi, K.H.; Koo, H.W.; Kim, T.W.; Kim, H.K. Antireflective ZnSnO/Ag bilayer-based transparent source and drain electrodes for transparent thin film transistors. *Appl. Phys. Lett.* **2012**, *100*, 263505. [CrossRef]
17. Moriga, T.; Hayashi, Y.; Kondo, K.; Nishimura, Y.; Murai, K.; Nakabayashi, I.; Fukumoto, H.; Tominaga, K. Transparent conducting amorphous Zn–Sn–O films deposited by simultaneous dc sputtering. *J. Vac. Sci. Technol. A* **2004**, *22*, 1705–1710. [CrossRef]
18. Huang, G.; Duan, L.; Dong, G.; Zhang, D.; Qiu, Y. High-mobility solution-processed tin oxide thin-film transistors with high-κ alumina dielectric working in enhancement mode. *ACS Appl. Mater. Interfaces* **2014**, *6*, 20786–20794. [CrossRef]
19. Alshammari, F.H.; Hota, M.K.; Wang, Z.; Al-jawhari, H.; Alshareef, H.N. Atomic-Layer-Deposited SnO_2 as Gate Electrode for Indium-Free Transparent Electronics. *Adv. Electron. Mater.* **2017**, *3*, 1700155. [CrossRef]
20. Morales-Masis, M.; Dauzou, F.; Jeangros, Q.; Dabirian, A.; Lifka, H.; Gierth, R.; Ruske, M.; Moet, D.; Hessler-Wyser, A.; Ballif, C. An indium-free anode for large-area flexible OLEDs: Defect-free transparent conductive zinc tin oxide. *Adv. Funct. Mater.* **2016**, *26*, 384–392. [CrossRef]
21. Um, D.S.; Woo, J.C.; Kim, C.I. Etching characteristics of TaN thin film using an inductively coupled plasma. *Surf. Coat. Technol.* **2010**, *205*, S333–S336. [CrossRef]
22. Ratcliff, E.L.; Sigdel, A.K.; Macech, M.R.; Nebesny, K.; Lee, P.A.; Ginley, D.S.; Armstrong, N.R.; Berry, J.J. Surface composition, work function, and electrochemical characteristics of gallium-doped zinc oxide. *Thin Solid Films* **2012**, *520*, 5652–5663. [CrossRef]
23. Sugiyama, K.; Ishii, H.; Ouchi, Y.; Seki, K. Dependence of indium–tin–oxide work function on surface cleaning method as studied by ultraviolet and x-ray photoemission spectroscopies. *J. Appl. Phys.* **2000**, *87*, 295–298. [CrossRef]
24. Shin, H.; Kim, C.; Bae, C.; Lee, J.S.; Lee, J.; Kim, S. Effects of ion damage on the surface of ITO films during plasma treatment. *Appl. Surf. Sci.* **2007**, *253*, 8928–8932. [CrossRef]

25. Masterton, W.L.; Slowinski, E.J.; Stanitski, C.L. *Chemical Principles: Alternative Edition with a Qualitative Analysis Supplement*; Saunders College Pub: Philadelphia, PA, USA, 1983.
26. D'Agostino, D.; Giorgio, C.D.; Bobba, F.; Trolio, A.D.; Alippi, P.; Cucolo, A.M.; Bonapasta, A.A. Effects of cobalt substitution on ZnO surface reactivity and electronic structure. *J. Mater. Chem. C* **2019**, *7*, 8364–8373. [CrossRef]
27. Gutmann, S.; Conrad, M.; Wolak, M.A.; Beerbom, M.M.; Schlaf, R. Work function measurements on nano-crystalline zinc oxide surfaces. *J. Appl. Phys.* **2012**, *111*, 123710. [CrossRef]
28. Zhang, X.; Qin, J.; Xue, Y.; Yu, P.; Zhang, B.; Wang, L.; Liu, R. Effect of aspect ratio and surface defects on the photocatalytic activity of ZnO nanorods. *Sci. Rep.* **2014**, *4*, 4596. [CrossRef]
29. Hu, X.; Masuda, Y.; Ohji, T.; Kato, K. Fabrication of $Zn(OH)_2$/ZnO nanosheet-ZnO nanoarray hybrid structured films by a dissolution-recrystallization route. *J. Am. Ceram. Soc.* **2010**, *93*, 881–886. [CrossRef]
30. Hwang, S.; Kim, Y.Y.; Lee, J.H.; Seo, D.K.; Lee, J.Y.; Cho, H.K. Irregular electrical conduction types in tin oxide thin films induced by nanoscale phase separation. *J. Am. Ceram. Soc.* **2012**, *95*, 324–327. [CrossRef]
31. Kover, L.; Kovacs, Z.; Sanjines, R.; Moretti, G.; Cserny, I.; Margaritondo, G.; Palinkas, J.; Adachi, H. Electronic structure of tin oxides: High-resolution study of XPS and Auger spectra. *Surf. Interface Anal.* **1995**, *23*, 461–466. [CrossRef]
32. Gamsjäger, H.; Gajda, T.; Sangster, J.; Saxena, S.K.; Voigt, W.; Perrone, J. *Chemical Thermodynamics of TIN*; OECD Publishing: Paris, France, 2012; Volume 12.
33. Reisman, A.; Berkenblit, M.; Ghez, R.; Chan, S.A. The equilibrium constant for the reaction of ZnO + H_2 and the chemical vapor transport of ZnO via the Zn + H_2O reaction. *J. Electron. Mater.* **1972**, *1*, 395–419. [CrossRef]
34. Liang, Z.; Zhang, Q.; Wiranwetchayan, O.; Xi, J.; Yang, Z.; Park, K.; Li, C.; Cao, G. Effects of the morphology of a ZnO buffer layer on the photovoltaic performance of inverted polymer solar cells. *Adv. Funct. Mater.* **2012**, *22*, 2194–2201. [CrossRef]